Supporting Information

Comparative Evaluation of MAX, MXene, NanoMAX and NanoMAX-derived-MXene for Microwave Absorption and Li ion Battery Anode Applications

Arundhati Sengupta,[†,a] B. V. Bhaskara Rao,[†,b] Neha Sharma,[a] Swati Parmar,[a] Vinila Chavan,[a] Sachin Kumar Singh,[a] Sangeeta Kale,[,b] and Satishchandra Ogale*[,a]*

a. Department of Physics and Centre for Energy Science, Indian Institute of Science Education and Research (IISER) Pune, Maharashtra-411008, India.

b. Defence Institute of Advanced Technology, Pune, Maharashtra-411025, India.

c. Research Institute for Sustainable Energy (RISE), TCG Centres for Research and Education in Science and Technology (TCG-CREST), 16th Floor, Omega, BIPL Building, Blocks EP & GP, Sector V, Salt Lake, Kolkata 700091, India.

† These authors have contributed equally to the work.

Experimental details

Synthesis of bulk Ti_3AlC_2 (MAX) and derived $Ti_3C_2T_x$ (MXene)

Ti_3AlC_2 MAX phase was synthesized by first ball-milling a mixture of Ti, Al and TiC powders (1:1.5:2 molar ratio) at 100 rpm for 24 h in Ar atmosphere and then heating the mixture in a covered alumina crucible at 1400 °C for 2 h in Ar atmosphere as per standard protocols.[1] The as-synthesized Ti_3AlC_2 was pulverized into a powder and used for measurements.

The MAX powder was sieved through a 400-mesh stainless steel sieve and treated with LiF-HCl (1.35 g LiF in 20 mL 12 M HCl used for ~2 g MAX) for 96 h with stirring at 300 rpm (at 35 °C) in a Teflon container. Thereafter, the $Ti_3C_2T_x$ MXene product so obtained in acidic solution was diluted with sufficient amount of water and separated with repeated centrifugation at 3500 rpm until the pH of the supernatant was ~ 6 and the product was no longer properly separable by means of centrifugation. At this point, vacuum filtration was used to separate out the product. The partly dried $Ti_3C_2T_x$ was then redispersed in water and sonicated for 30 min in an ice-cooled water-bath with continuous Ar bubbling through the dispersion. The dispersion was allowed to stand for 15 min and the supernatant was centrifuged at 1000 rpm. The supernatant solution from this centrifugation contained $Ti_3C_2T_x$ sheets freed from residual Ti_3AlC_2 and these $Ti_3C_2T_x$ MXene sheets were finally collected by vacuum filtration, dried under vacuum at room temperature and stored for measurements.

Synthesis of nanostructured Ti_3AlC_2 (NanoMAX) and derived $Ti_3C_2T_x$ (MXene-N)

Bulk Ti_3AlC_2 was ball-milled for 24 h at 350 rpm to obtain nanostructured Ti_3AlC_2 powder, denoted NanoMAX. This NanoMAX powder was subjected to the same treatment with LiF-HCl as described in the case of synthesis of MXene sheets (96 h with stirring at 300 rpm at 35 °C). The obtained $Ti_3C_2T_x$ (MXene-N) product in acidic solution was diluted with sufficient amount of water and separated with repeated centrifugation at 5000 rpm until the pH of the supernatant was ~ 6 and the product was no longer properly separable by means of centrifugation. At this stage, the centrifuge tubes were gently shaken to redisperse the MXene-N and a final round of centrifugation at 500 rpm was carried out to ensure removal of any residual Ti_3AlC_2 from the supernatant solution which is subsequently vacuum filtered to collect the final MXene-N product which is used for measurements.

Material characterization techniques

Structure and phases of different samples were studied using X-ray diffraction (XRD) patterns recorded on a Bruker D8 Advance X-ray diffractometer in scanning mode at 40 kV and 30 mA using Cu Kα radiation (λ = 1.5406 Å). Field emission scanning electron microscope (FESEM) at 3 kV (FEI NOVA NANO SEM) was used to study the microstructure. High resolution transmission electron microscope (HRTEM) operating at an accelerating voltage of 200 kV (JEOL JEM-2200FS) was used to study the microstructure of selected samples (powder dispersed in water, drop-cast and dried on a holey carbon-coated Cu TEM grid). Raman spectroscopy measurements were carried out with a RENISHAW spectrometer instrument using a 532 nm laser source. The Fourier transform infrared spectroscopy (FTIR) was done using a NICOLET 6700 FTIR spectrophotometer. X-ray photoelectron spectroscopy (XPS) was performed on K ALPHA + Thermo Fisher Scientific Instruments having X-ray source of Al K Alfa (Monochromatic) with 6 mA beam current and 12 kV.

Microwave absorption measurement details

Microwave absorption property of material is measured with help of one port VNA (model PNA Network Analyzer N5222A ranging from 10 MHz–26.5 GHz (Agilent)) by Reflection Loss (RL) measurement. Absorption or RL property of material measured using X-Band (8.2-12.4 GHz) wave guide of 1 Port VNA with corresponding metal backing placed after the material. RL is the logarithmic ratio of impedances of the free space and air - absorber, expressed in decibels (dB).

$$Reflection\ Loss\ (RL) = 20\ log\ [\frac{Z_1 - Z_0}{Z_1 + Z_0}]$$

where $$Z_1 = Z_0(\frac{\mu_r}{\varepsilon_r})^{\frac{1}{2}} tanh[j(\frac{2\pi f d}{C})(\mu_r \varepsilon_r)^{\frac{1}{2}}]$$

where $Z_0 \sim 377\ \Omega$ is the free space impedance and Z_1 is Impedance of air-absorber interface, and $\varepsilon_r = \varepsilon' - \varphi\varepsilon''$ is permittivity and $\mu_r = \mu' - j\ \mu''$ is permeability of material. When thickness of absorbing material $t = m\lambda/4$, $m = 1,2,3\ldots$then input and reflected waves are out of phase, thus there is no reflection at the air-absorber interface.

Another key parameter for electromagnetic absorption materials is that the skin depth, which is described as the distance in the material "δ" over which the amplitude of a travelling plane wave decreases by a factor e^{-1}, can be expressed as $\delta = 1/(\pi f \mu \sigma)^{1/2}$, where f is frequency of microwave wave and σ is conductivity of material.[2-6]

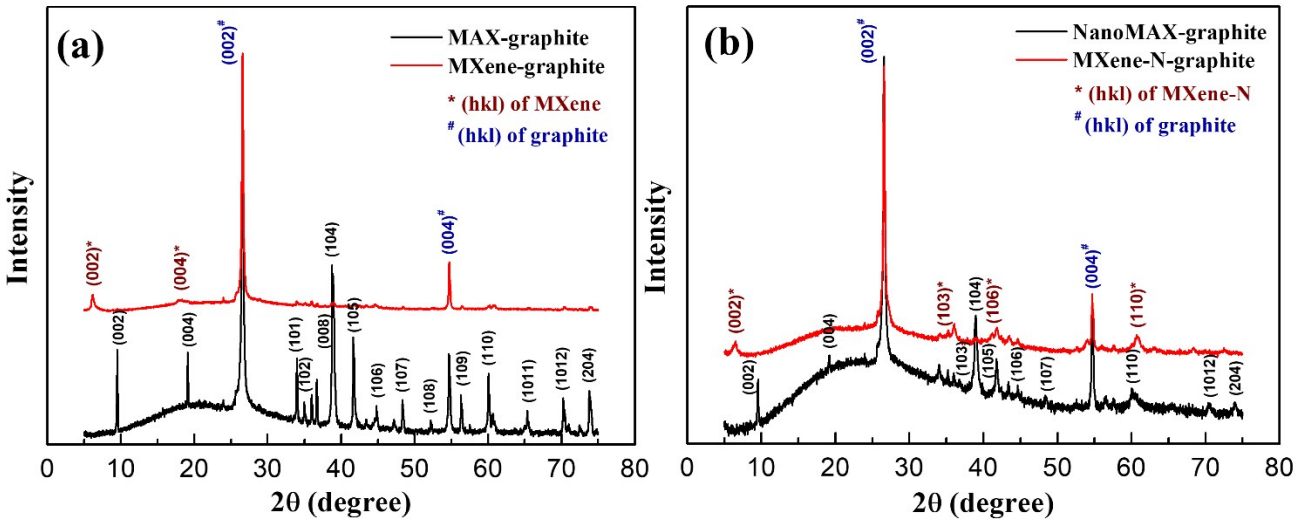

Figure S1: XRD patterns of a) MAX-graphite and MXene-graphite, and b) NanoMAX-graphite and MXene-N-graphite paints coated on PET sheet.

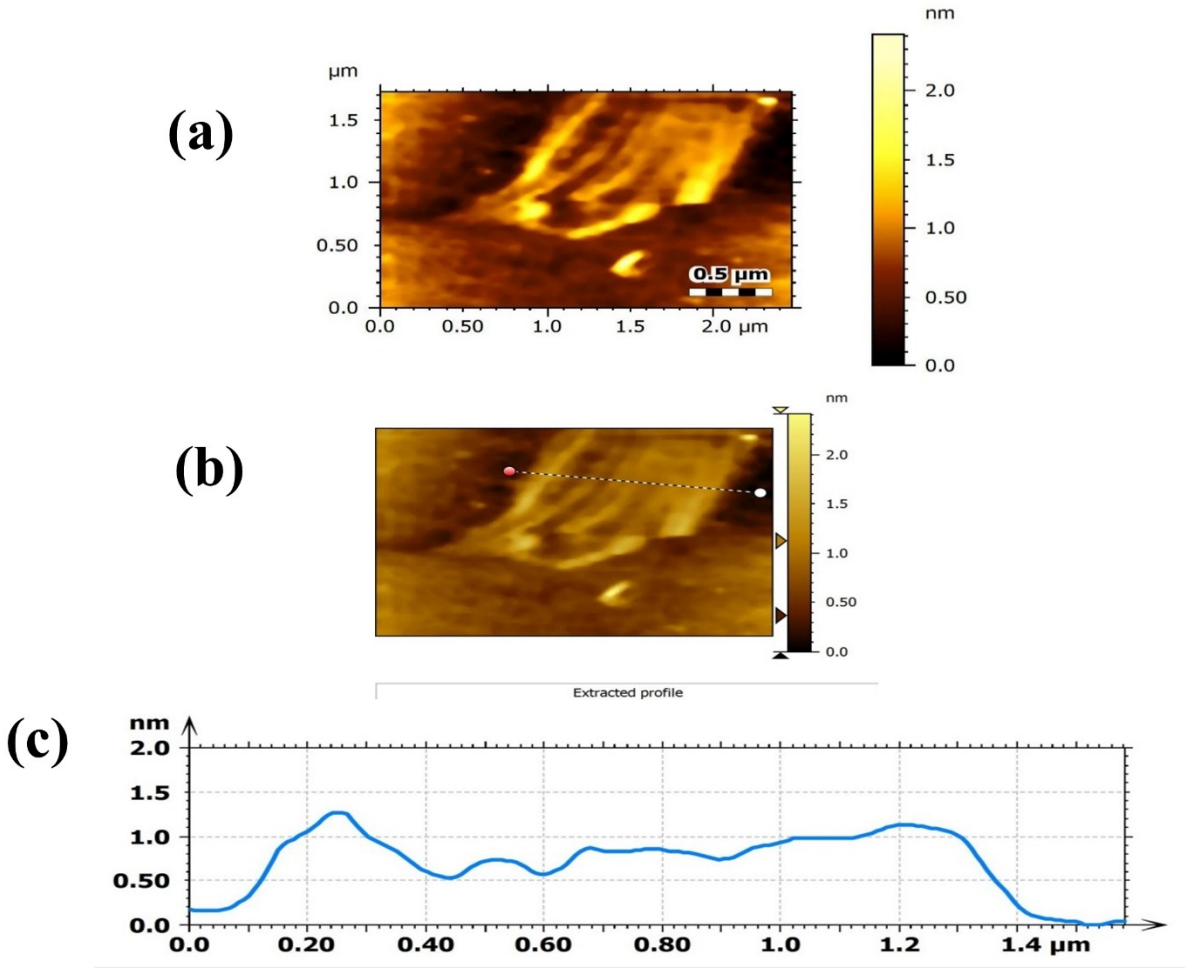

Figure S2: (a,b) AFM image of a typical exfoliated MXene sheet, with (c) the cross-width and height shown along the marked line in (b).

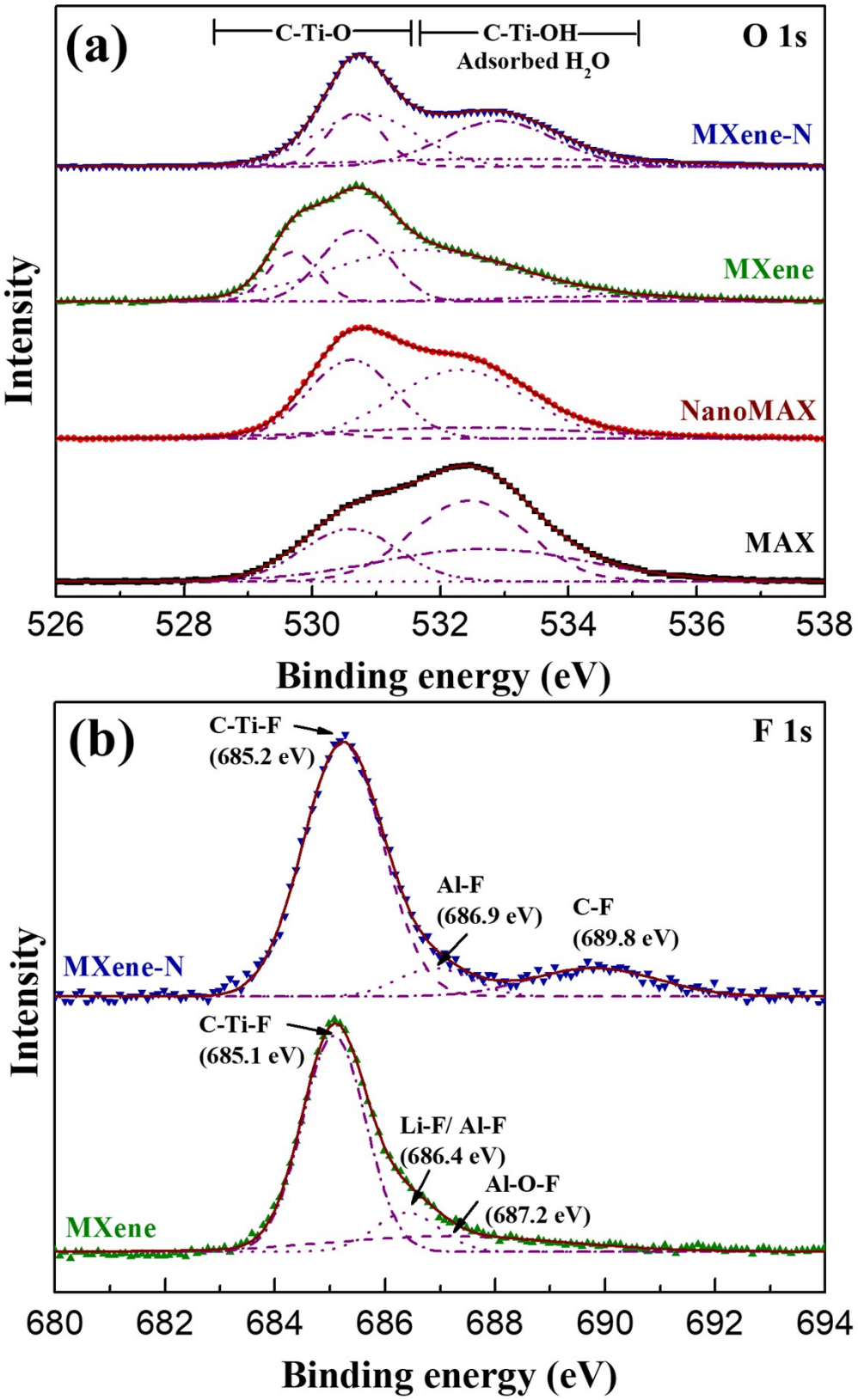

Figure S3: XPS spectra of a) O 1s levels of MAX, NanoMAX, MXene, and MXene-N, and b) F 1s levels of MXene and MXene-N.

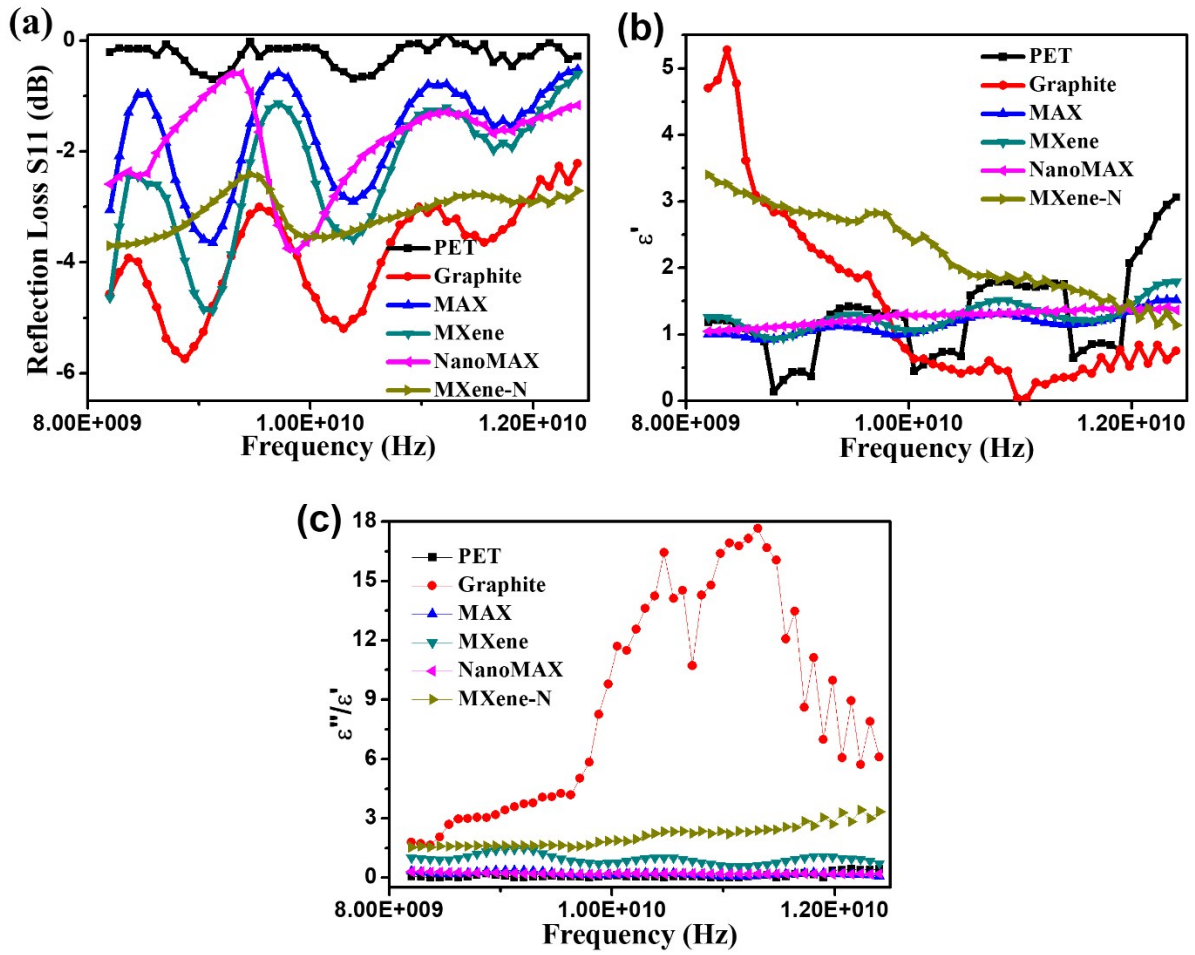

Figure S4: Individual components of composites like PET, graphite, MAX, MXene, NanoMAX, and MXene-N responses of a) Reflection Loss (dB), b) Real part of dielectric constant, and c) Loss Tangent.

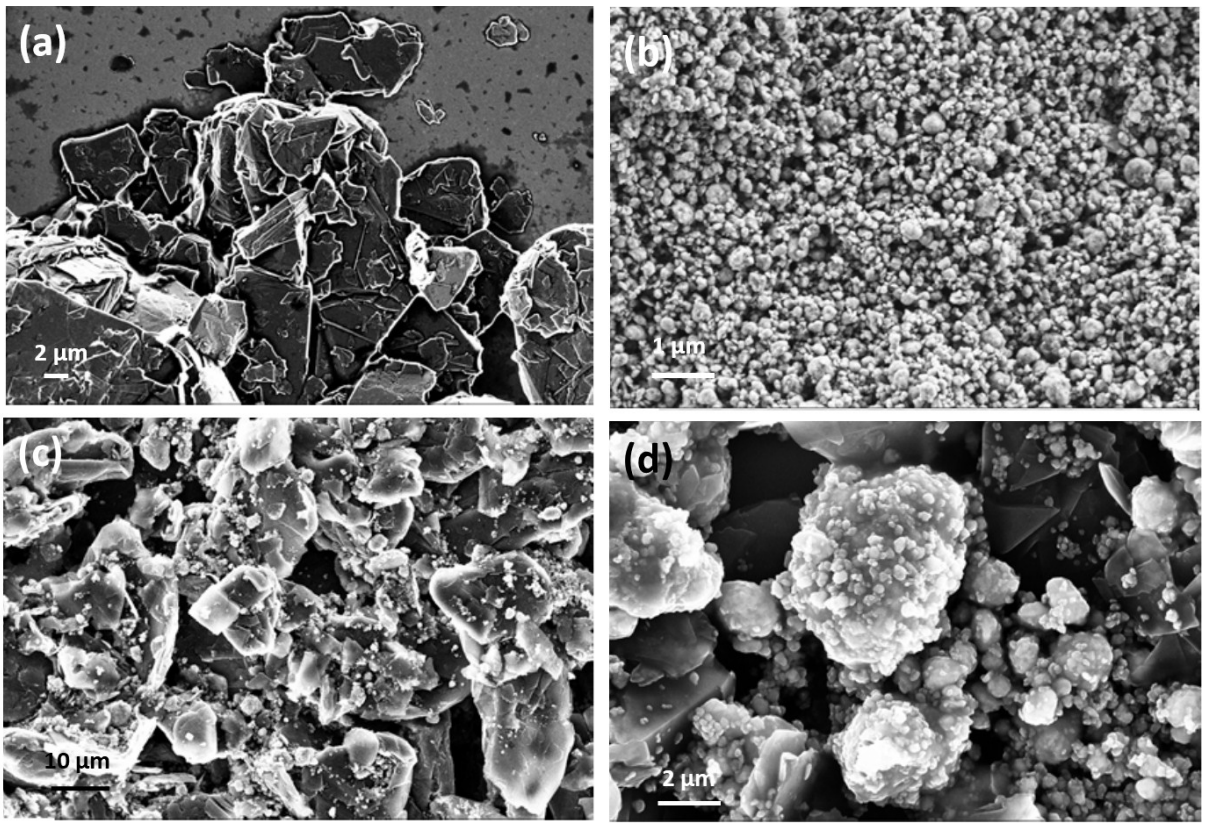

Figure S5: FESEM images of a) Graphite flakes, b) NanoMAX, c) and d) NanoMAX- Graphite composite film.

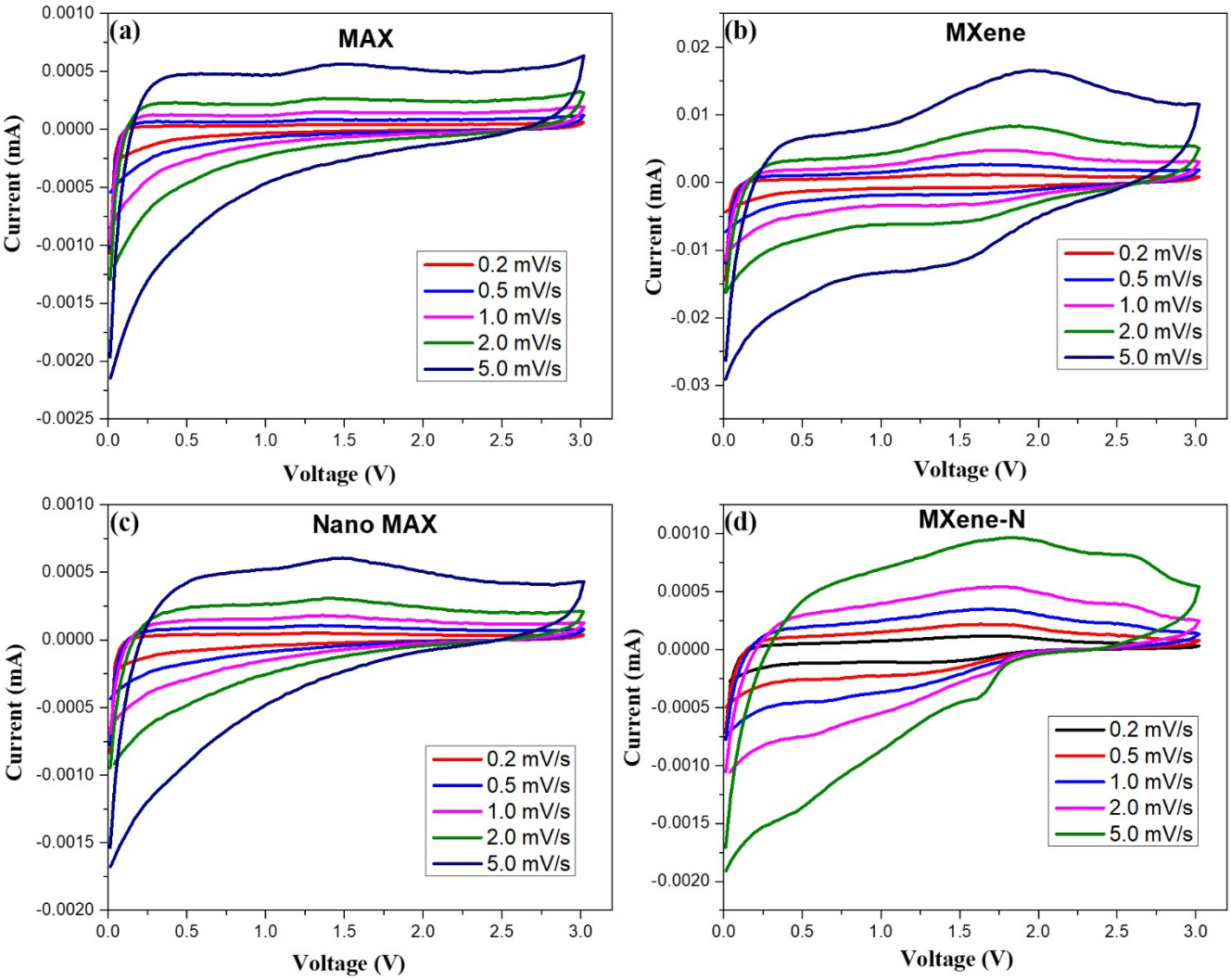

Figure S6: Multi scan rate cyclic voltammograms of (a) MAX, (b) MXene, (c) NanoMAX and (d) MXene-N in the range of 0.01 to 3.0 V w.r.t. Li/Li^+.

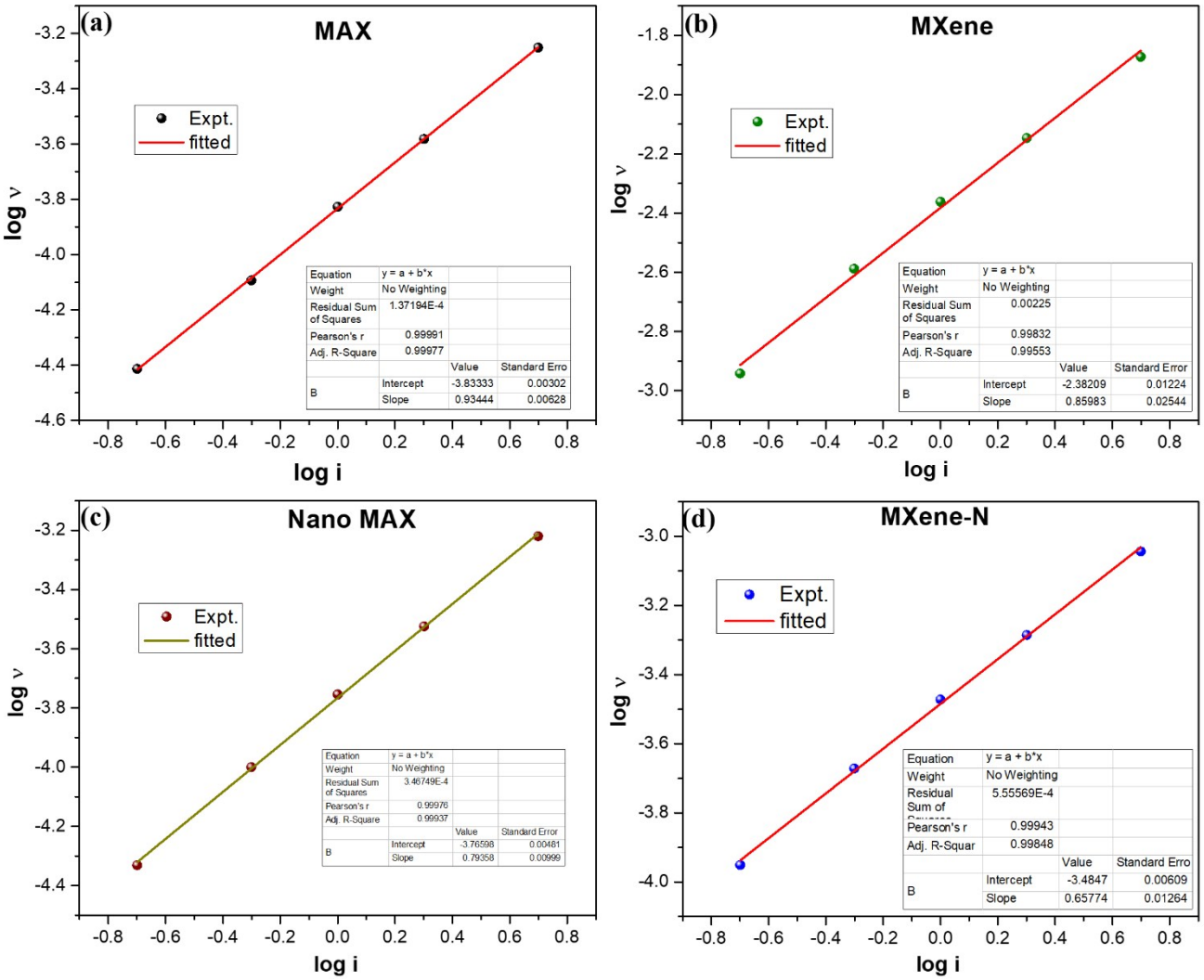

Figure S7: log i vs. log ν plot of (a) MAX, (b) MXene, (c) NanoMAX and (d) MXene-N.

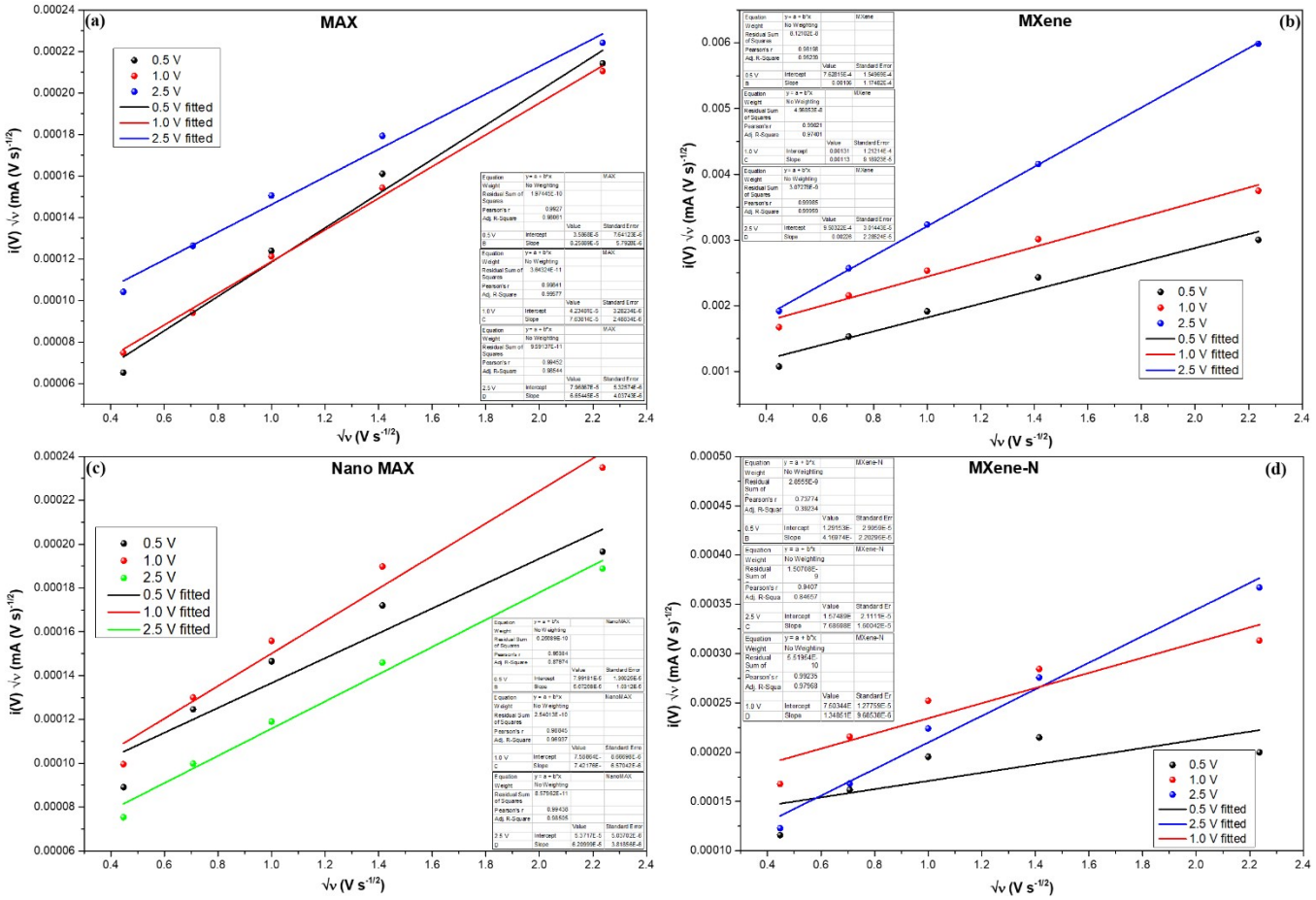

Figure S8: i(V)/√ν vs. √ν plot of (a) MAX, (b) MXene, (c) NanoMAX and (d) MXene-N.

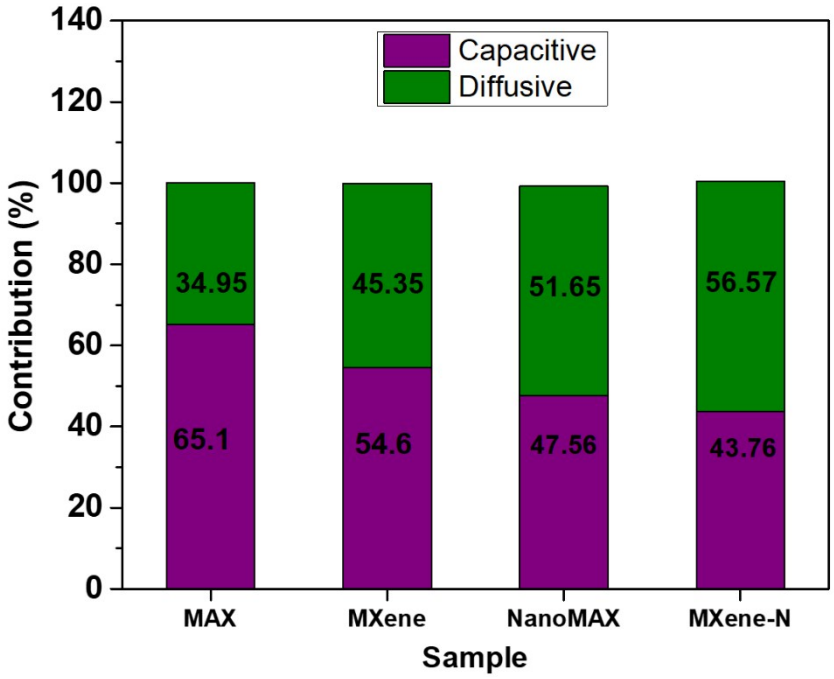

Figure S8: Estimation of diffusive and capacitive contributions of all the samples.

Determination of the charge-discharge behavior: To gain a better understanding of the mechanism of the charge discharge behavior and to determine the quantitative analysis of diffusive and capacitive contributions, cyclic voltammetry was carried out at different scan rates as shown in Figure S6 for all the four samples under study namely MAX, Mxene, NanoMAX, Mxene-N. From these plots, MAX is found to have majorly intercalation type behaviour but other three samples are seen to show some diffusive charater at around 2.0 V and 1.5 V. The scan rate dependence of CV current can be expressed by the power law[7]:

$$i(V) = a\nu^b$$

where i (V) is the current, a and b are constant parameters and ν is the scan rate. The value of b can be determined from the slope of log (i) vs. log (ν) plot in Figure S7 and it gives a good indication on the nature of the charge storage.[7] For diffusion controlled process, b is 0.5 and for capacitive behavior b should be equal to 1. Here we find that except MXene-N, other three samples exhibit majorly the capacitive charge discharge behavior since the b value lies within the range of 0.8 to 1 for these three samples. The ratio of capacitive behavior decreases from MAX to NanoMAX and diffusion process dominates in Mxene-N with the b-value of 0.65774.

The total amount of current for reactions involving diffusive and capacitive contribution at any fixed potential can be calculated using the following equation[7]:

$$i(V) = s_1\nu + s_2\sqrt{\nu}$$

Here, s_1 and s_2 are constants corresponding to the capacitive and diffusive currents, respectively. These constants can be estimated from the $i(V)/\sqrt{\nu}$ vs $\sqrt{\nu}$ plot where s_1 and s_2 can be estimated from the slope and the intercept, respectively.[8] Figure S8 illustrates the same at different voltages for all the samples. From this, the ratio of capacitive and diffusive current at a given potential can be calculated, as illustrated in Figure S9. This calculation also corroborates with the b-values showing capacitive behavior dominance in MAX which decreases from MXene, NanoMAX to MXene-N.

Table S1: Comparison of reversible capacity and stability of different MXenes and MXene-derivatives used as anode material in LIB.

Anode material for LIB	C-rate or Current density	Cycle number	Reversible capacity (mAh g^{-1})	References
Ti_2C	1C	80	110	[9]
Delaminated Ti_3C_2 "paper"	1C	100	410	[10]
Ti_3C_2 (HF-exfoliated) Ti_3C_2 intercalated with DMSO (after HF-exfoliation)	1C 1C	75 75	90 119	[11]
Ti_2CT_x partially oxidized in H_2O_2	100 mA g^{-1}	50	389	[12]
Free standing $Ti_3C_2T_x$	1C	500	~100	[13]
Ti_3CNT_x nanosheets (Freeze-dried)	0.5 A g^{-1}	1000	300	[14]
Ti_3C_2 multilayer Ti_3C_2 (vacuum-calcined at 400 °C) Ti_3C_2 (vacuum-calcined at 700 °C)	1C 1C 1C	100 100 100	87 126 147	[15]
$Ti_3C_2T_x$ (O-rich)	100 mA g^{-1}	500	404	[16]
$Ti_3C_2T_x$ fluorinated for 24 h (2D layered $TiOF_2$ phase)	1C	500	~110	[17]
Nb_2CT_x V_2CT_x	1C 1C	150 150	170 260	[18]
$Mo_2TiC_2T_x$ 'paper'	1C	160	~145	[19]
Nb_2CT_x (few layer)	1 A g^{-1}	800	225	[20]
Nitrogen doped Nb_2CT_x	0.2C 0.5C	100 1500	360 288	[21]
$Nb_4C_3T_x$	100 mA g^{-1}	100	310	[22]
$Nb_4C_3T_x$ partially oxidized in CO_2 (850 °C, 0.5 h)	0.25C 1C	400 400	208 167	[23]
MXene-N ($Ti_3C_2T_x$ nanoparticles)	100 mA g^{-1}	1000	330	This work

References

[1] M. Alhabeb, K. Maleski, B. Anasori, P. Lelyukh, L. Clark, S. Sin, Y. Gogotsi, *Chem. Mater.* **2017**, *29*, 7633.

[2] M. B. Amin, J. R. James, *Radio and Electronic Engineer* **1981**, 51, 209.

[3] K. K. Gupta, S. M. Abbas, T. H. Goswami, A. C. Abhyankar, *J. Magn. Magn. Mater.* **2014**, *362*, 216.

[4] A. Xie, F. Wu, M. Sun, X. Dai, Z. Xu, Y. Qiu, Y. Wang, M. Wang, *Appl. Phys. Lett.* **2015**, *106*, 222902.

[5] B. V. B. Rao, P. Yadav, R. Aepuru, H. S. Panda, S. Ogale, S. N. Kale, *Phys. Chem. Chem. Phys.* **2015**, *17*, 18353.

[6] B. V. B. Rao, N. Kale, B. S. Kothavale, S. N. Kale, *AIP Advances*, **2016,** *6*, 065107.

[7] K. V. Sankar, R. K. Selvan, *J. Power Sources* **2015**, *275*, 399.

[8] V. Augustyn, P. Simon, B. Dunn, *Energy Environ. Sci.* **2014**, *7* (5), 1597.

[9] M. Naguib, J. Come, B. Dyatkin, V. Presser, P.-L. Taberna, P. Simon, M. W. Barsoum, Y. Gogotsi, *Electrochem. Commun.* **2012**, *16*, 61.

[10] O. Mashtalir, M. Naguib, V. N. Mochalin, Y. Dall'Agnese, M. Heon, M. W. Barsoum, Y. Gogotsi, *Nat. Commun.* **2013**, *4*, 1716.

[11] D. Sun, M. Wang, Z. Li, G. Fan, L.-Z. Fan, and A. Zhou, *Electrochem. Commun.*, **2014**, *47*, 80–83.

[12] B. Ahmed, D. H. Anjum, M. N. Hedhili, Y. Gogotsi, H. N. Alshareef, *Nanoscale*, **2016**, *8*, 7580.

[13] H. Zhang, X. Xin, H. Liu, H. Huang, N. Chen, Y. Xie, W. Deng, C. Guo, W. Yang, *J. Phys. Chem. C* **2019**, *123*, 2792.

[14] F. Du, H. Tang, L. Pan, T. Zhang, H. Li, J. Xiong, J. Yang, C. Zhang, *Electrochim. Acta*, **2017**, *235*, 690.

[15] F. Kong, X. He, Q. Liu, X. Qi, Y. Zheng, R. Wang, Y. Bai, *Electrochim. Acta* **2018**, *265*, 140.

[16] Y. Wang, C. Ma, W. Ma, W. Fan, Y. Sun, H. Yin, X. Shi, X. Liu, Y. Ding, *2D Mater.* **2019**, *6*, 045025.

[17] B. P. Thapaliya, C. J. Jafta, H. Lyu, J. Xia, H. M. Meyer, M. P. Paranthaman, X.-G. Sun, C. A. Bridges, S. Dai, *Chem. Sus. Chem.* **2019**, *12*, 1316.

[18] M. Naguib, J. Halim, J. Lu, K. M. Cook, L. Hultman, Y. Gogotsi, M. W. Barsoum*, J. Am. Chem. Soc.* **2013**, *135*, 15966.

[19] B. Anasori, Y. Xie, M. Beidaghi, J. Lu, B. C. Hosler, L. Hultman, P. R. C. Kent, Y. Gogotsi, M. W. Barsoum, *ACS Nano* **2015**, *9*, 9507.

[20] J. Zhao, J. Wen, L. Bai, J. Xiao, R. Zheng, X. Shan, L. Li, H. Gao, X. Zhang, *Dalton Trans.* **2019**, *48*, 14433.

[21] R. Liu, W. Cao, D. Han, Y. Mo, H. Zeng, H. Yang, W. Li, *J. Alloys Compds.* **2019**, *793*, 505.

[22] S. Zhao, X. Meng, K. Zhu, F. Du, G. Chen, Y. Wei, Y. Gogotsi, Y. Gao, *Energy Storage Mater.* **2017**, *8*, 42.

[23] C. Zhang, S. J. Kim, M. Ghidiu, M.-Q. Zhao, M. W. Barsoum, V. Nicolosi, Y. Gogotsi, *Adv. Funct. Mater.* **2016**, *26*, 4143.